Observation of electron–hole puddles in graphene using a scanning single-electron transistor

J. MARTIN[1], N. AKERMAN[1], G. ULBRICHT[2], T. LOHMANN[2], J. H. SMET[2], K. VON KLITZING[2] AND A. YACOBY[1,3]*

[1]Department of Condensed Matter Physics, Weizmann Institute of Science, Rehovot 76100, Israel
[2]Max-Planck-Institut für Festkörperforschung, Heisenbergstrasse 1, D-70569 Stuttgart, Germany
[3]Department of Physics, Harvard University, Cambridge, Massachusetts 02138, USA
*e-mail: yacoby@physics.harvard.edu

Published online: 25 November 2007; doi:10.1038/nphys781

The electronic structure of graphene causes its charge carriers to behave like relativistic particles. For a perfect graphene sheet free from impurities and disorder, the Fermi energy lies at the so-called 'Dirac point', where the density of electronic states vanishes. But in the inevitable presence of disorder, theory predicts that equally probable regions of electron-rich and hole-rich puddles will arise. These puddles could explain graphene's anomalous non-zero minimal conductivity at zero average carrier density. Here, we use a scanning single-electron transistor to map the local density of states and the carrier density landscape in the vicinity of the neutrality point. Our results confirm the existence of electron–hole puddles, and rule out extrinsic substrate effects as explanations for their emergence and topology. Moreover, we find that, unlike non-relativistic particles the density of states can be quantitatively accounted for by considering non-interacting electrons and holes.

The kinetic energy of Dirac particles in graphene increases linearly with momentum[1–5]. The total energy per particle however, also referred to as the chemical potential, μ, contains further exchange and correlation contributions that arise from the Coulomb interaction $\mu = E_K + E_{ex} + E_c$ (refs 6–11). Here, E_K, E_{ex} and E_c are the kinetic, exchange and correlation terms respectively. Therefore, the chemical potential and its derivative with respect to density provide direct insight into the properties of the Coulomb interaction in such a system. The derivative is known as the inverse compressibility (that is, the inverse of the density of states). Compressibility measurements of conventional, massive, two-dimensional (2D) electron systems made for example of Si or GaAs have been carried out by several groups[8,12–15]. For these 2D systems it has been shown that at zero magnetic field, the chemical potential may be described accurately within the Hartree–Fock approximation. Quantitatively, Coulomb interactions add a substantial negative contribution to the compressibility and become dominant at low carrier densities. Although transport measurements in graphene indicate high mobilities even at low carrier densities[16–18], many questions pertaining to disorder[19–30] remain unanswered. In a perfectly uniform and clean graphene sample, the inverse compressibility is expected to diverge at the Dirac point in view of the vanishing density of states. This divergence, however, is expected to be rounded off by disorder on length scales smaller than our spatial resolution. Long-range disorder on the other hand will cause local shifts in the Dirac point indicative of a non-zero local density. Here, we measure the spatial dependence of the local compressibility versus carrier density across the sample. Fluctuations in the Dirac point across the sample are translated into carrier density maps through which quantitative information about the degree and length scale of disorder is obtained.

The preparation of graphene monolayers is carried out in a similar manner as in refs 16,31. We use Nitto tape to peel a large graphite flake from a highly oriented pyrolytic graphite crystal and press it onto a Si/SiO_2 wafer. The conducting Si substrate serves as a back-gate to vary the carrier density in the graphene sheet[16]. Once a suitable monolayer is selected in an optical microscope, two electrical contacts to the layer are patterned with optical lithography. Typical dimensions of our monolayers are $10 \times 4\,\mu m^2$. After lift-off of the ohmic contact metal (3 nm Cr, 30 nm Au), the graphene flakes typically exhibit their neutrality point at back-gate voltages larger than 100 V. Therefore, the sample surface is cleaned by an ozone treatment and an ammonia dip. As-prepared flakes typically have their neutrality point at back-gate voltages of around 30 V. The sample is then mounted in the preparation chamber of the ultrahigh-vacuum scanning system and subsequently annealed by heating it above 100 °C at a background pressure of 5×10^{-7} mbar. The entire annealing procedure apparently removes most of the doping adsorbates introduced during fabrication and water, as the neutrality point shifts close to zero back-gate voltage[32]. A back-gate voltage difference of 1 V corresponds to a density change of $7 \times 10^{10}\,cm^{-2}$. This conversion factor has been extracted from magnetotransport data (Fig. 1a). The unorthodox Hall quantization in graphene monolayers allows us to distinguish them from multilayer flakes[17,18]. Figure 1a shows the two-terminal conductance G_{2pt} as a function of density and magnetic field. Maxima in G_{2pt} can be clearly seen at

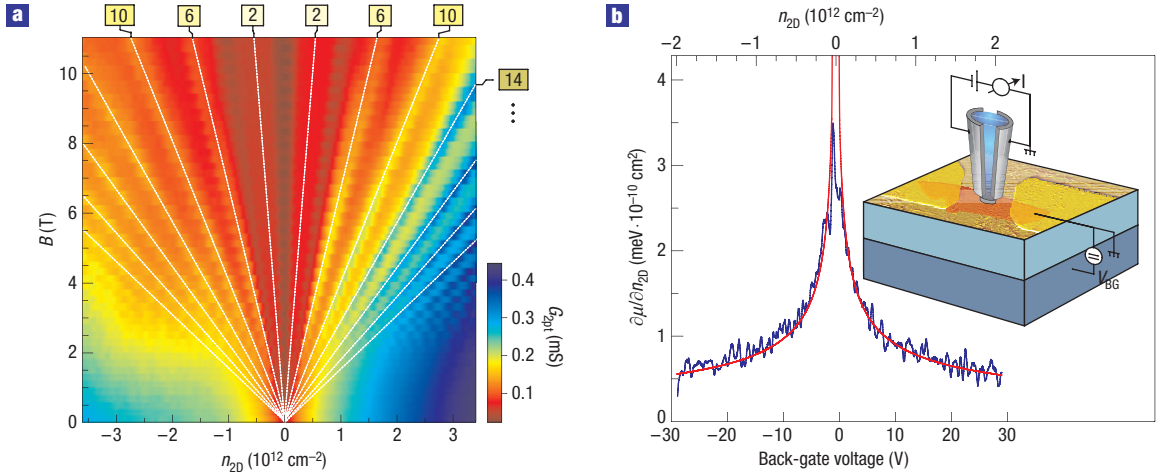

Figure 1 Characterization of a graphene monolayer with transport and inverse compressibility measurements. a, Colour rendering of the two-terminal conductance G_{2pt} of a graphene monolayer in the density versus magnetic field plane. The conductance maxima follow slopes corresponding to integer fillings of 2, 6, 10 and so on, an unequivocal signature for a single monolayer. **b**, The inverse compressibility measured at an arbitrary fixed location on the graphene sample as a function of the back-gate voltage or carrier density (blue line). The red line is a best fit to the data using an effective Fermi velocity as a single fit parameter in the kinetic energy contribution predicted from the graphene band structure. The inset shows the experimental arrangement consisting of an aluminium-based SET evaporated on a glass-fibre tip of a scanning probe microscope. The graphene monolayer is contacted with two leads (typically 10 μm apart) on top of an oxidized and heavily doped Si wafer. A back-gate voltage induces charge carriers and modulates the density for the measurement of the local compressibility.

filling factors of 2, 6, 10 and so on for both electrons and holes. This behaviour conclusively identifies the flake as a monolayer.

The local compressibility measurements of graphene described here are carried out using a scanable single-electron transistor (SET). Previous scanning tunnelling microscopy (STM) studies on bulk graphite surfaces in strong magnetic fields already demonstrated the power of local methods to probe this class of materials[33–35]. Recently, atomic-resolution STM and non-contact atomic force microscopy studies on graphene flakes were reported. These studies revealed, among other things, the atomic structure of graphene and structural corrugations that partially conform to the underlying silicon oxide[36]. Scanning tunnelling spectroscopy studies were also carried out on epitaxially grown graphene on silicon carbide substrates. These studies highlighted in-plane defects as a dominant source of backscattering[37]. Unlike STM, which probes the single-particle density of states, the inverse compressibility, addressed here, measures the many-body density of states that includes information on the exchange and correlation energies as well. The experiments are carried out at 0.3 K. A schematic diagram of the experimental set-up is shown in the inset to Fig. 1b. Details of our experimental method are described in refs 38,39. The diameter of the SET is about 100 nm and the distance between the SET and the sample is roughly 50 nm. The SET tip is capable of measuring the local electrostatic potential with microvolt sensitivity and a high spatial resolution close to its size. The inverse compressibility can be measured by monitoring the change in the local electrostatic potential, Φ_{total}, when modulating the carrier density in the graphene flake with the back-gate, $\partial\Phi_{\mathrm{total}}/\partial n$. We note that the small size of the graphene flake requires us to consider position-dependent direct pick-up from the fringing electric fields between the back-gate plane and the graphene flake as discussed in Supplementary Information part A. In the absence of any transport current, any change in the local electrostatic potential is equal in magnitude and opposite in sign to the changes in the local chemical potential of the graphene, $e(\partial\Phi_{\mathrm{total}}/\partial n) = -\partial\mu/\partial n$. Figure 1b shows the inverse compressibility for a fixed location of the SET as a function of the back-gate voltage at zero magnetic field.

On the basis of the linear dispersion of the graphene band structure, the kinetic energy contribution to the inverse compressibility is expected to exhibit an unusual density dependence with a singularity at the neutrality point given by $\hbar v_{\mathrm{F}} \cdot \sqrt{\pi/|n|g_s}$. Here v_{F} is the Fermi velocity, g_s is the band degeneracy and $|n|$ is the carrier density measured from the neutrality point. At zero magnetic field $g_s = 4$ owing to both spin and band symmetries. The maximum in the experimental $\partial\mu/\partial n$ trace clearly identifies the position of the Dirac point at this particular location. The absence of a singularity at the Dirac point in the experiment is ascribed to disorder broadening. As the kinetic term in graphene has the same density dependence as the leading exchange and correlation terms, it is instructive to fit the data to the kinetic term with a single fit parameter that may be thought of as an effective Fermi velocity. The red line in Fig. 1b shows the result of such a fit and yields $v_{\mathrm{F}}^{\mathrm{eff}} = 1.1 \times 10^6 \pm 0.1 \times 10^6$ m s^{-1}. The indicated uncertainty reflects the accuracy with which the direct pick-up correction can be carried out. It is noteworthy that infrared spectroscopy studies of Landau levels in graphene also obtained a band velocity of about 1.1×10^6 m s^{-1} (ref. 40). The velocity increase compared with band-structure calculations, which predict $v_{\mathrm{F}} = 1 \times 10^6$ m s^{-1}, was attributed to electron–electron correlations. Here, the predicted band-structure value[1] lies within our experimental uncertainty and so we conclude that the compressibility data can be described quantitatively by the kinetic term alone. The exchange and correlation contributions to the compressibility are either weak or cancel each other out. Theory too has suggested only weak modifications of the compressibility due to exchange[9–11]. This is in marked contrast to massive 2D systems such as GaAs where at low densities the exchange term dominates[8,12–14]. Moreover, in these conventional 2D electron systems, quantitative agreement between experiment and theory is only accomplished when taking into account the non-zero thickness of the 2D layer[8,13]. The finite width is responsible for a softening of the Coulomb interaction between the electrons as well as a Stark-like shift of the confinement energies in the potential well when the density is tuned. Both effects produce non-generic changes to the compressibility terms, which depend on

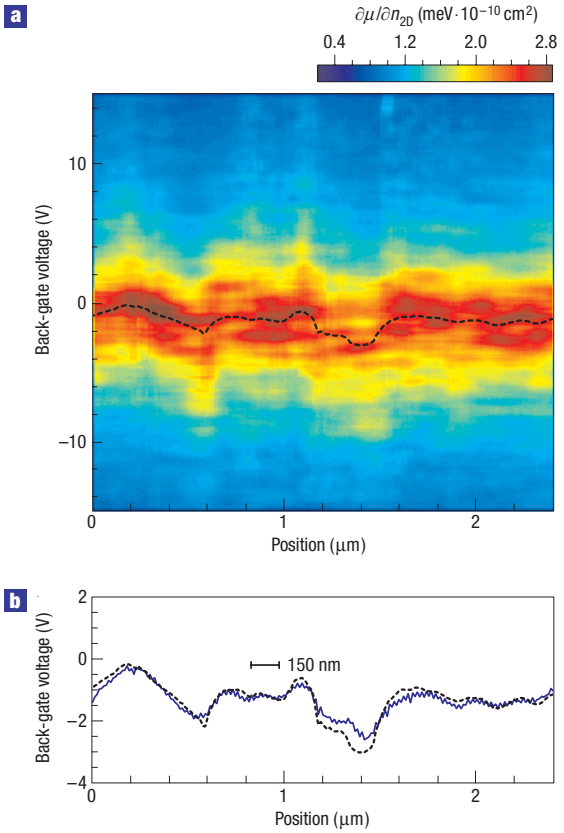

Figure 2 The Dirac point measured as a function of position. a, Colour rendering of the inverse compressibility measured along a line across the sample as a function of the back-gate voltage. The dashed black line marks the location of the Dirac point obtained from a fit of the kinetic energy term to each line scan. **b**, Comparison of the spatial variation of the Dirac point extracted using two methods: the inverse compressibility (black dashed line, identical to the dashed line in **a**) and through subtracting surface potential scans at high and zero average carrier density (blue line). The bar marks the smallest length scale (approximately 150 nm) on which density variations are observed.

the details of the heterostructure. These complications however do not arise for graphene as its thickness is negligible.

The peaked behaviour of the inverse compressibility as a function of back-gate voltage or density may be used to map out the density fluctuations in the graphene sheet. At different locations across the sample, the local density is added to the externally induced density by the back-gate. Therefore, different back-gate voltages are required to zero the density at each location and reach the Dirac point. In practice this means that the entire inverse compressibility curve is shifted along the back-gate voltage axis as we move from one point across the sample to another. Figure 2a shows a measurement of the inverse compressibility along an arbitrarily chosen line across the sample. The Dirac point is located within the red coloured band, which corresponds to reduced compressibility. As expected, it appears at different back-gate voltages for different locations. The black dashed line shows the dependence of the Dirac point on position, obtained by fitting the kinetic term of the compressibility to each back-gate voltage line scan. The smallest length scale on which density variations are observed is roughly 150 nm. This scale is most likely limited by our spatial resolution, that is, the size of the SET. The underlying density fluctuations are therefore bound to occur on even smaller length scales and with higher amplitudes. Direct evidence for that is given below.

The chemical potential variations within the graphene are probably due to charged impurities above and below the layer. In the process of scanning the SET above the layer, we pick up not only the spatial variations in the chemical potential but also the potential emanating directly from the charges above the layer along with their image charges in the layer. As these potentials are much larger than the chemical potential variations it would be desirable to find means to subtract them and be left with only the chemical potential variations. This can be readily achieved by subtracting the measured potential at zero average density from that at a high carrier density. As the carrier density in the graphene sheet increases it is expected to screen better. Hence, at large carrier density, the potential landscape in the graphene should be nearly constant and the only potential seen by the SET is that due to static charges above the layer. Using this method, we can extract the local carrier density from the measurements of the surface potential alone. A formal description of this subtraction process, which validates this method, is given in Supplementary Information part B. Figure 2b shows a comparison of the density variations as extracted from the inverse compressibility measurements (black dashed line, which is identical to the one in Fig. 2a) with those extracted from the surface potential (blue solid line). There is striking quantitative agreement between the two methods. Figure 3a shows a 2D map of the density variations of the graphene sheet when the average carrier density is zero. It was obtained from surface potential measurements. The red regions correspond to electrons and the blue regions correspond to holes. These data constitute direct evidence for the puddle model[25,41]. These puddles may account for the anomalous minimal conductivity observed at zero average density[42–44]. A statistical analysis of the density fluctuations present in this 2D map is shown in Fig. 3b. The histogram plots the number of patches in which the density lies within a certain density interval. From the standard deviation of a fit with a gaussian distribution, we extract that the density fluctuations are of the order of $\Delta n_{2D,B=0\,T} = \pm 3.9 \times 10^{10}\,\mathrm{cm}^{-2}$.

To verify the influence of the substrate on the disorder landscape observed in graphene, potential fluctuations were recorded as seen by the SET on a nearby patch of the bare silicon oxide surface. An example of a 2D scan is shown in Fig. 4a when the SET scanning tip is placed at a distance of approximately 150 nm from the bare silicon oxide surface. This distance is slightly larger that the distance used to image the surface of graphene (50 nm). The distance primarily affects the spatial resolution and for a random potential landscape the r.m.s. value will appear smaller by the square root of the change in area (namely another factor of 1.5, as our resolution is limited to about 100 nm at short distances). Figure 4b shows a histogram of the potential distribution across the scanned region. A gaussian fit to the distribution yields a variance of 50 mV. This corresponds to a variation in the electron charge on the SET island of approximately $1/2e$. This is obtained from the charge periodicity of the SET in the present configuration where 100 mV of back-gate voltage is needed to add a single electron to the SET. Had the graphene monolayer been there instead of the SET, similar charge variations would have been induced in it. To determine the corresponding density variations, we estimate the effective area integrated by the SET. The distance of the SET from the surface sets a lower bound on the substrate area probed by it and we conclude that $2 \times 10^9\,\mathrm{cm}^{-2}$ represents an upper limit for the density fluctuations caused by trapped charges within the oxide or at the oxide surface. We find a value very similar to the above value in measurements of the bare substrate potential that are taken at a closer distance

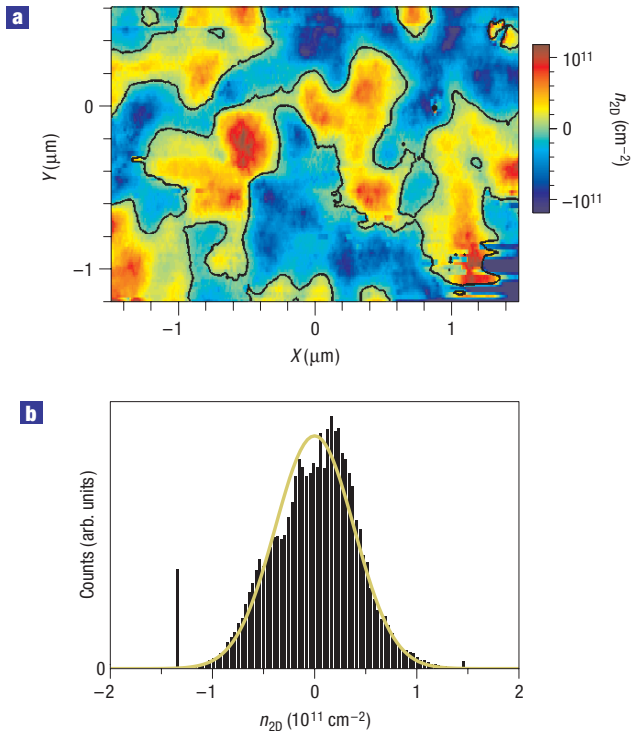

Figure 3 Spatial density fluctuations and electron/hole puddles. a, Colour map of the spatial density variations in the graphene flake extracted from surface potential measurements at high density and when the average carrier density is zero. The blue regions correspond to holes and the red regions to electrons. The black contour marks the zero density contour. **b**, Histogram of the density distribution in **a**.

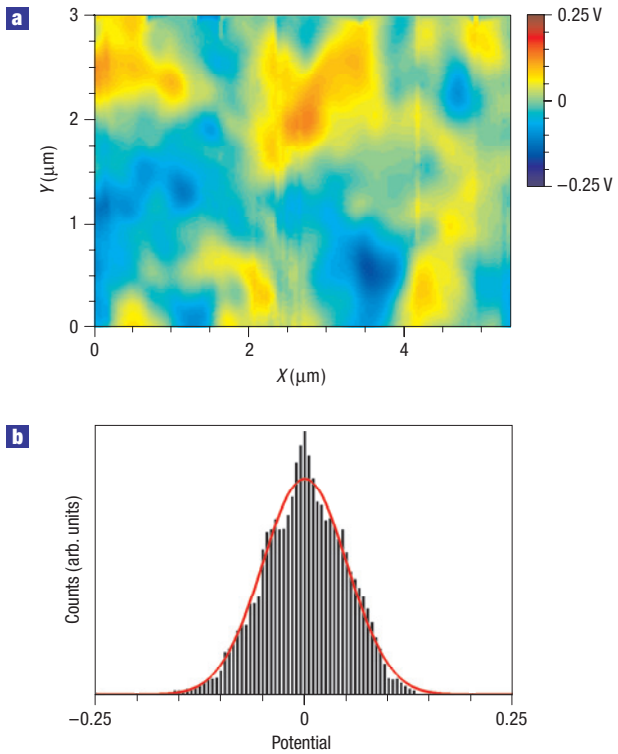

Figure 4 Potential variations on the substrate. a, Colour map of the spatial fluctuations in the surface potential measured above a patch of the bare silicon oxide surface near the graphene flake. **b**, Histogram of the potential fluctuation distribution in **a**. The variance is approximately equal to 50 mV.

similar to the distance used when imaging the compressibility of the graphene layer. This result suggests that density fluctuations in graphene do not primarily originate from trapped oxide charge. Studies of the nanoscale morphology of silicon oxide and graphene using non-contact atomic force microscopy have revealed that the graphene flake partially conforms to substrate corrugations and that without further treatment acrylic resists used in the fabrication may leave a residue on the graphene flake[36]. Both substrate-induced structural distortions as well as chemical doping from resist residue are conceivable sources of density fluctuations. Even though our sample was not exposed to an acrylic resist, we cannot exclude that photoresist too leaves a residue despite ozone and ammonia treatment. In addition, atmospheric species trapped in between the flake and substrate as well as chemical adsorbants on top of the flake may represent an important source of disorder, even though the large shift of the neutrality point on annealing in vacuum indicates that these chemical absorbates can to a large extent be removed. STM studies on epitaxial graphene grown on SiC suggested in-plane defects as an important source of disorder[37]. It is beyond the scope of this work to identify the precise origin of disorder. Instead, this work intends to unveil the typical characteristics of density fluctuations present in graphene flakes obtained through mechanical exfoliation procedures and with similar quality to the ones used in previously reported transport and spectroscopy studies of graphene.

The fluctuations in density discussed thus far have been resolution limited by our technique. However, the intrinsic density fluctuations may be extracted by going into the quantum Hall regime (intrinsic here is used synonymously with not resolution smeared). A large magnetic field applied perpendicular to the sample produces bands of localized and extended states that are manifested in universal transport properties[45]. Our previous studies on GaAs 2D electron systems have shown that at sufficiently large magnetic fields, the width in density of the band of localized states, also referred to as the incompressible band, becomes field and also filling factor independent. This width constitutes a direct measure of the density fluctuations in the sample[46]. Figure 5 shows a colour rendering of the $\partial\mu/\partial n$ measured on our graphene flake as a function of the magnetic field and density. A single density scan at the fixed field of 11 T is shown in Fig. 5b. It is composed of a series of maxima at the integer fillings 2, 6, 10 and so on, corresponding to regions of low compressibility. These maxima can be fitted well by gaussians of identical variance, which is in accordance with the filling-independent width of the incompressible bands observed in conventional 2D systems. The variance may serve as a measure for the disorder amplitude. A best fit to the data is obtained assuming density fluctuations of approximately $\Delta n_{2D,B=11\,T} = \pm 2.3 \times 10^{11}\,\mathrm{cm}^{-2}$. A similar analysis at lower magnetic fields shows that the variance still drops slightly with decreasing magnetic field and hence the value $\Delta n_{2D,B=11\,T}$ is a lower bound for the disorder strength as bands of localized states are not well separated yet. The disorder amplitude extracted from these measurements in the presence of a magnetic field is about a factor of six larger than the disorder estimate $\Delta n_{2D,B=0\,T}$ from the $B = 0$ T measurement in Fig. 3. This difference allows us to deduce the intrinsic disorder length scale, l_{disorder}. For the zero field estimate, the density fluctuations are averaged over an area determined by the tip size with a characteristic dimension of approximately 150 nm (see Fig. 2b). The ratio of these averaged density fluctuations and the intrinsic ones is simply the square root of the ratio of the

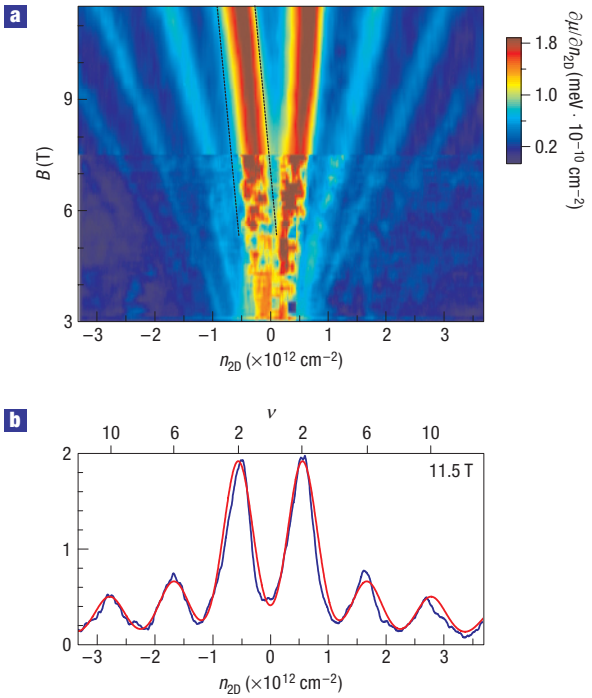

Figure 5 Estimate of the disorder from high magnetic field measurements. **a**, Colour rendering of the inverse compressibility as a function of density and magnetic field. The black dashed lines demarcate the incompressible band centred around filling factor 2. The incompressible band maintains a constant width as the magnetic field and density increase. **b**, A single line scan from plot **a** of the measured inverse compressibility (blue line) at a magnetic field of 11 T. The red curve is a fit to the data composed of gaussians with equal variance for each maximum. This variance measures the width of the incompressible regions (maxima) centred around integer fillings and provides an estimate for the intrinsic amplitude of the density fluctuations.

disorder area to the averaged area. Therefore, we end up with an upper bound for the intrinsic disorder length scale of about 30 nm. We note as a curiosity that a similar number is obtained from the Einstein relation between conductivity and compressibility, $\sigma = e^2 D(\partial n/\partial\mu)$, for the mean free path when plugging in the expression for the diffusion constant valid for conventional 2D systems: $D = v_F l/2$. Here, l is the mean free path. The conductivity near the neutrality point is approximately $\sigma \approx 4e^2/h$ and $\partial n/\partial\mu$ is shown in Fig. 1.

We conclude that the intrinsic disorder length scale in graphene is approximately 30 nm. Whereas at high carrier density the high compressibility of graphene smooths out the disorder landscape, screening becomes poor and the intrinsic disorder length becomes relevant as we approach the neutrality point. A carrier landscape with co-existing electron and hole puddles emerges. Hence, charge carriers are omnipresent despite vanishing average carrier density, which may provide the most natural explanation for the minimal conductivity and Hall resistance behaviour near the neutrality point reported in graphene transport studies[42–44].

Received 21 May 2007; accepted 8 October 2007; published 25 November 2007.

References

1. Brandt, N. B., Chudinov, S. M. & Ponomarev, Y. G. *Semimetals 1, Graphite and Its Compounds* (North-Holland, Amsterdam, 1988).
2. Semenoff, G. W. Condensed-matter simulation of a three dimensional anomaly. *Phys. Rev. Lett.* **53**, 2449–2452 (1984).
3. Haldane, F. D. M. Model for a quantum Hall effect without Landau levels: Condensed-matter realization of the "parity anomaly". *Phys. Rev. Lett.* **61**, 2015–2018 (1988).
4. Zhou, S. Y. *et al.* First direct observation of Dirac fermions in graphite. *Nature Phys.* **2**, 595–599 (2006).
5. Bostwick, A., Ohta, T., Seyller, T., Horn, K. & Rotenberg, E. Quasiparticle dynamics in graphene. *Nature Phys.* **3**, 36–40 (2007).
6. Fetter, A. L. & Walecka, J. D. *Quantum Theory of Many Particle Systems* (McGraw-Hill, New York, 1971).
7. Bello, M. S., Levin, E. I., Shklovskii, B. I. & Efros, A. L. Density of localized states in the surface impurity band of a metal-insulator-semiconductor structure. *Sov. Phys. JETP* **53**, 822–829 (1981).
8. Eisenstein, J. P., Pfeiffer, L. N. & West, K. W. Compressibility of the two-dimensional electron gas: Measurements of the zero-field exchange energy and fractional quantum Hall gap. *Phys. Rev. B* **50**, 1760–1778 (1994).
9. Peres, N. M. R., Guinea, F. & Castro Neto, A. H. Coulomb interactions and ferromagnetism in pure and doped graphene. *Phys. Rev. B* **72**, 174406 (2005).
10. Barlas, Y., Pereg-Barnea, T., Polini, M., Asgari, R. & MacDonald, A. H. Chirality and correlations in graphene. *Phys. Rev. Lett.* **98**, 236601–236604 (2007).
11. Hwang, E. H., Hu, B. Y.-K. & Das Sarma, S. Density dependent exchange contribution to $\delta\mu/\delta n$ in extrinsic graphene. Preprint at <http://www.arxiv.org/cond-mat/0703499v1> (2007).
12. Eisenstein, J. P., Pfeiffer, L. N. & West, K. W. Negative compressibility of interacting two-dimensional electron and quasiparticle gases. *Phys. Rev. Lett.* **68**, 674–677 (1992).
13. Millard, S. *et al.* Effect of finite quantum well width on the compressibility of a two-dimensional electron gas. *Phys. Rev. B* **55**, 6715–1618 (1997).
14. Shapira, S. *et al.* Thermodynamics of a charged fermion layer at high r_s values. *Phys. Rev. Lett.* **77**, 3181–3184 (1996).
15. Kravchenko, S. V., Ringberg, D. A., Semenchinsky, S. G. & Pudalov, V. M. Evidence for the influence of electron–electron interaction on the chemical potential of the two-dimensional electron gas. *Phys. Rev. B* **42**, 3741–3744 (1990).
16. Novoselov, K. S. *et al.* Electric field effect in atomically thin carbon films. *Science* **306**, 666–669 (2004).
17. Novoselov, K. S. *et al.* Two dimensional gas of massless Dirac fermions in graphene. *Nature* **438**, 197–200 (2005).
18. Zhang, Y., Tan, Y.-W., Stormer, H. L. & Kim, P. Experimental observation of the quantum Hall effect and Berry's phase in graphene. *Nature* **438**, 201–204 (2005).
19. Peres, N. M. R., Guinea, F. & Castro Neto, A. H. Electronic properties of disordered two-dimensional carbon. *Phys. Rev. B* **73**, 125411 (2006).
20. Sheng, D. N., Sheng, L. & Sheng, Z. Y. Quantum Hall effect in graphene: disorder effect and phase diagram. *Phys. Rev. B* **73**, 233406 (2006).
21. Khveschenko, D. V. Electron localization properties in graphene. *Phys. Rev. Lett.* **97**, 036802–036805 (2006).
22. Ziegler, K. Robust transport properties in graphene. *Phys. Rev. Lett.* **97**, 266802–266805 (2006).
23. Ostrovsky, P. M., Gornyi, I. V. & Mirlin, A. D. Electron transport in disordered graphene. *Phys. Rev. B* **74**, 235443 (2006).
24. Aleiner, I. L. & Efetov, K. B. Effect of disorder on transport in graphene. *Phys. Rev. Lett.* **97**, 236801–236804 (2006).
25. Hwang, E. H., Adam, S. & Das Sarma, S. Carrier transport in two-dimensional graphene layers. *Phys. Rev. Lett.* **98**, 186806–186809 (2007).
26. Nomura, K. & MacDonald, A. H. Quantum transport of massless Dirac fermions in graphene. *Phys. Rev. Lett.* **98**, 076602–076605 (2007).
27. Cheianov, V. & Fal'ko, V. I. Friedel oscillations, impurity scattering and temperature dependence of resistivity in graphene. *Phys. Rev. Lett.* **97**, 226801–226804 (2006).
28. McCann, E. *et al.* Weak-localization magnetoresistance and valley symmetry in graphene. *Phys. Rev. Lett.* **97**, 146805–146809 (2006).
29. Gonzales, J., Guinea, F. & Vozmediano, M. A. H. Electron–electron interactions in graphene sheets. *Phys. Rev. B.* **63**, 134421 (2001).
30. Castro Neto, A. H. & Kim, E.-A. Charge inhomogeneity and the structure of graphene sheets. Preprint at <http://www.arxiv.org/cond-mat/0702562v1> (2007).
31. Novoselov, K. S. *et al.* Two-dimensional atomic crystals. *Proc. Natl Acad. Sci. USA* **102**, 10451–10453 (2005).
32. Schedin, F. *et al.* Detection of individual gas molecules adsorbed on graphene. *Nature Mater.* **6**, 652–655 (2007).
33. Matsui, T. *et al.* STS observations of Landau levels at graphite surfaces. *Phys. Rev. Lett.* **94**, 226403–226406 (2005).
34. Niimi, Y., Kambara, H., Matsui, T., Yoshioka, D. & Fukuyama, H. Real-space imaging of alternate localization and extension of quasi-two-dimensional electronic states at graphite surfaces in magnetic fields. *Phys. Rev. Lett.* **97**, 236804–236807 (2006).
35. Niimi, Y. *et al.* Scanning tunneling microscopy and spectroscopy of the electronic local density of states of graphite surfaces near monoatomic step edges. *Phys. Rev. B* **73**, 085421 (2006).
36. Ishigami, M., Chen, J. H., Cullen, W. G., Fuhrer, M. S. & Williams, E. D. Atomic structure of graphene on SiO_2. *Nano Lett.* **7**, 1643–1648 (2007).
37. Rutter, G. M. *et al.* Scattering and interference in epitaxial graphene. *Science* **317**, 219–222 (2007).
38. Yoo, M. J. *et al.* Scanning single-electron transistor microscopy: Imaging individual charges. *Science* **276**, 579–582 (1997).
39. Yacoby, A., Hess, H. F., Fulton, T. A., Pfeiffer, L. N. & West, K. W. Electrical imaging of the quantum Hall state. *Solid State Commun.* **111**, 1–13 (1999).
40. Jiang, Z. *et al.* Infrared spectroscopy of Landau levels of graphene. *Phys. Rev. Lett.* **98**, 197403–197407 (2007).
41. Cheianov, V. V., Fal'ko, V. I., Altschuler, B. L. & Aleiner, I. L. Random resistor network model of minimal conductivity in graphene. *Phys. Rev. Lett.* **99**, 176801 (2007).
42. Geim, A. K. & Novoselov, K. S. The rise of graphene. *Nature Mater.* **6**, 183–191 (2007).
43. Katnelson, M. I., Novoselov, K. S. & Geim, A. K. Chiral tunnelling and the Klein paradox in graphene. *Nature Phys.* **2**, 620–625 (2006).
44. Cho, S. & Fuhrer, M. S. Charge transport and inhomogeneity near the charge neutrality point in graphene. Preprint at <http://www.arxiv.org/abs/0705.3239> (2007).
45. Prange, R. E. & Girvin, S. M. *The Quantum Hall Effect* (Springer, New York, 1990).
46. Ilani, S. *et al.* The microscopic nature of localization in the quantum Hall effect. *Nature* **427**, 328–332 (2004).

Acknowledgements

We acknowledge helpful discussions on the preparation of graphene flakes with K. Novoselov and A. Geim. We would also like to acknowledge fruitful discussions with F. von Oppen.
Correspondence and requests for materials should be addressed to A.Y.
Supplementary Information accompanies this paper on www.nature.com/naturephysics.